A hybrid source of quantum light for generation of frequency tunable Fock states

Aleksa Krstić,[1, *] Priyanshu Tiwari,[1] Florian Höhe,[2] Frank
Setzpfandt,[1, 3] Ulf Peschel,[4] Joachim Ankerhold,[2] and Sina Saravi[1]

[1]*Institute of Applied Physics, Abbe Center of Photonics,*
Friedrich-Schiller University Jena, Albert-Einstein-Straße 15, 07745 Jena, Germany
[2]*Institute for Complex Quantum Systems and IQST,*
University of Ulm, Albert-Einstein-Allee 11, 89069 Ulm, Germany
[3]*Fraunhofer Institute for Applied Optics and Precision Engineering, Albert-Einstein-Straße 7, 07745 Jena, Germany*
[4]*Institute of Condensed Matter Theory and Solid State Optics,*
Friedrich-Schiller University Jena, Max-Wien-Platz 1, 07743 Jena, Germany
(Dated: April 25, 2024)

We propose a scheme for quantum-light generation in a nonlinear cavity hybridized with a 2-level system. We theoretically show that, when excited by a series of controlled pump pulses, the hybrid source can generate various Fock states with high probabilities, such as near-on-demand generation of 1- and 2-photon states, and above 50% probability for generation of Fock states with up to 7 photons. More importantly, the tailorable nature of the nonlinear cavity and its pumping allows for generating Fock states with arbitrary frequencies, even with a fixed 2-level system, creating fundamentally new opportunities in all areas of quantum technologies.

Introduction.

To support the realization of optical quantum technologies [1–4], development of efficient and tailorable sources of quantum light, such as squeezed light and Fock states, is of major interest. While squeezed light can reliably be generated using nonlinear parametric processes [5, 6], generation of optical Fock states with photon numbers $n \geq 2$ is notoriously difficult in practice and is an ongoing topic of research. The majority of proposals and implementations rely on either of the two general approaches: using atomic or atom-like solid-state quantum systems [7–10], with successful implementations mainly based on temporal demultiplexing of single photons from a single quantum dot [11–13], or using nonlinear parametric sources, where Fock states can be heralded by conditional measurement of squeezed-light states [14–16]. Yet both approaches have their limitations. Although capable of deterministic generation, atomic and solid-state systems have very limited tunabilities [17], especially in their spectra, which result in states with limited tailorability in spectral/modal properties.

In contrast, nonlinear sources are widely tunable in spectral, modal, and polarization degrees of freedom, specially in nanostructured platforms [18], yet they only generate Fock states probabilistically, with decreasing probability for higher photon-number states [16].

Motivated by these complementary advantages and disadvantages of nonlinear and atom-like systems, we aim for a hybrid system combining the two, that exploits both their advantages towards creating an ideal source of Fock states, one that is on-demand and tunable. Such hybrid systems have attracted attention recently, with proposals for enhancing atom-cavity interaction [19, 20], single-photon generation with enhanced purity [21], generating equally weighted superposition of Fock states [22], and generating Schrödinger cat states [23].

In this Letter, we propose a hybrid source, consisting of a nonlinear cavity and a two-level system (2LS), for generation of Fock states with enhanced probabilities and arbitrary frequencies. To this end, we use a sequence of optical pump pulses for the nonlinear cavity, with controlled amplitudes, phases, and temporal delays, and leverage the complex interplay between squeezed-light generation and its interaction with a 2LS. Importantly, the properties of the generated Fock states, specially their frequency, can be adjusted by tuning the parameters of the nonlinear process. We also study this system's performance in the presence of cavity losses.

Basic principles. The hybrid source is depicted schematically in Fig. 1(a), in which a nonlinear crystal with second-order susceptibility $\chi^{(2)}$ and a 2LS, are embedded in an optical cavity. The nonlinear cavity, without the 2LS, when pumped by an optical field of frequency $\omega_p = \omega_s + \omega_i$, can generate two-mode squeezed vacuum (TMSV) into two separate resonance modes of the cavity, referred to as *signal* and *idler* modes, of frequencies ω_s and ω_i, respectively. The 2LS has the transition frequency ω_0, which is resonant with the idler mode, i.e., $\omega_i = \omega_0$. The TMSV state generated by the squeezing operator $e^{-i(r\hat{a}_i^\dagger \hat{a}_s^\dagger + \text{H.c.})}$ can be written as a superposition of perfectly photon-number correlated states as $|\text{TMSV}\rangle = \text{sech}\,\zeta \sum_{n=0}^{\infty}(i\,e^{i\phi}\tanh\zeta)^n|n,n\rangle$ [24, 25]. Here, $\hat{a}_i^\dagger$ and $\hat{a}_s^\dagger$ are the creation operators for the idler and signal modes, respectively. We adopt the convention that a state of the form $|m,n\rangle$ contains m idler, and n signal photons and also refer to states where $n = m$ as *multi-pair* states. Additionally, ζ and ϕ are the magnitude and phase, respectively, of the complex parametric gain $r = \zeta\,e^{i\phi}$, determined by the properties of the nonlinear cavity and the pump field [24].

In Fig. 1(b), we show the probability of finding the first few multi-pair states in a TMSV state, as a function of
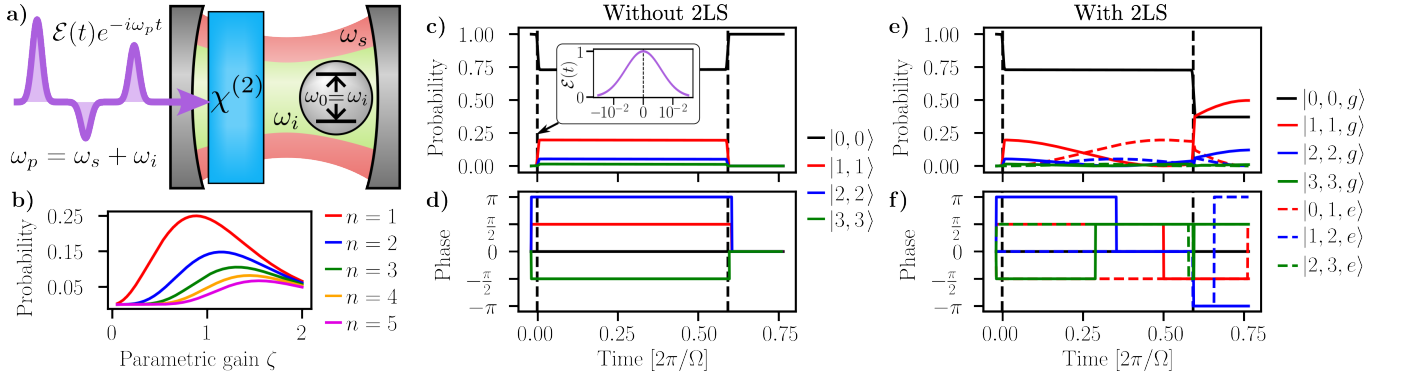
FIG. 1. **(a)** Schematic representation of the hybrid source. A sequence of pump pulses with distinct temporal separations, amplitudes, and phases are incident on a nonlinear cavity, to generate a two-mode squeezed vacuum (TMSV) in the signal and idler modes. Simultaneously, the idler photons undergo resonant Rabi oscillations with a 2LS. **(b)** Probabilities of obtaining the five lowest order $|n, n\rangle$ states as a function of a real-valued parametric gain r, in a conventional TMSV source without the 2LS. **(c,d)** Temporal evolution of the probabilities (c) and phases of probability amplitudes (w.r.t. the $|0, 0\rangle$ state) (d) for the three lowest order $|n, n\rangle$ in a configuration with two pump pulses and no 2LS. The pulses have the parametric gains $r_1 = -r_2 \approx 0.58$ and a temporal separation of $T_1 = 0.59 \frac{2\pi}{\Omega}$. Vertical black dashed lines indicate the arrival time of each pump pulse. As the pulses are too short to be discernible at these time scales, a plot of a pump pulse envelope is shown in the inset of (c); **(e,f)** Temporal evolution of a few lowest-order composite states $|n, n, g\rangle$ and $|n - 1, n, e\rangle$ (phases w.r.t. the $|0, 0, g\rangle$ state), in the nonlinear cavity with the 2LS, for the same pumping configuration as in (c,d).

the parametric gain. We observe that, as the parametric gain increases, these probabilities rise to a maximum value and then decrease. This is a consequence of lower-order $|n, n\rangle$ states "seeding" the generation of the higher-order ones. This property of squeezed-light sources sets a fundamental limit on the probability of generating any given multi-pair state. In principle, a combination of heralding and multiplexing approaches can be used to enhance the generation probability of a specific Fock state. Yet, this demands enormous resources in practice, even for the simplest case of realizing an on-demand source of single photons [26, 27].

Hybrid dynamics. The hybrid system dynamics can be described with the following Hamiltonian in the interaction picture, $\hat{H}(t) = \hbar \Gamma \mathcal{E}(t) \hat{a}_i^\dagger \hat{a}_s^\dagger + i\hbar \frac{\Omega}{2} \hat{a}_i \hat{\sigma}^\dagger + \text{H.c.}$ [28, 29]. Here, Γ is a nonlinear coupling constant, representing the nonlinear efficiency of the cavity for TMSV generation. Ω is the single-photon Rabi frequency, and $\hat{\sigma}$ is the atomic lowering operator for the 2LS. $\mathcal{E}(t)$ is the temporal envelope of the pump field, which is made of a sequence of temporally distinct pulses. Each pump pulse is enumerated by the number j, and is characterized by a parametric gain $r_j = \zeta_j \, e^{i\phi_j} = \Gamma \int_j \mathrm{d}t \, \mathcal{E}(t)$, where the integration extends over the duration of the j-th pulse. Without loss of generality, we use Gaussian pump pulses with temporal widths fixed to $\approx 5 \times 10^{-3} \frac{2\pi}{\Omega}$, much shorter than the temporal period of few-photon Rabi oscillations between the idler photons and the 2LS, which allows us to isolate the dynamics of nonlinear generations from the Rabi oscillations. Essentially, with every shot of a pump pulse, the nonlinear Hamiltonian induces a quick change in the system's state, followed by much slower Rabi oscillations. For numerical calculations, we also used `QuTiP` library in

Python [30]. The details of the analytical derivations and numerical procedures are outlined in the Supplementary [31].

To understand the hybrid dynamics, an example with a two-pulse pump sequence is shown in Fig. 1(c-f). We plot the temporal evolution of the first few multi-pair states, where we show their probabilities and their relative phases with respect to the $|0, 0\rangle$ state. In Fig. 1(c,d), we study the case of the nonlinear cavity without the 2LS, essentially a TMSV source. We use two pump pulses of equal gain magnitudes, but with a relative phase difference of π, with $r_1 = -r_2 \approx 0.58$. The sharp changes in all the plots correspond to the points in time where a pump pulse is incident on the nonlinear cavity. As we see in this case, these two pulses cancel each others parametric gains, resulting in a perfect destructive nonlinear interference [32], creating the TMSV with the first pulse and going back to the vacuum state with the second pulse. In Figs. 1(e,f), we show the results for the same two-pulse configuration as in Figs. 1(c,d), but now in the presence of the 2LS in the nonlinear cavity. Firstly, we see that for each individual multi-pair state generated by the first pump pulse, the hybrid system experiences Rabi oscillations between composite states $|n, n, g\rangle$ and $|n - 1, n, e\rangle$, where g (e) indicates the ground (excited) state of the 2LS. The frequency of each Rabi oscillation is proportional to $\sqrt{n}$ [28, 29]. This scaling of the Rabi frequency with photon number, results in a complex set of relative phases between individual multi-pair states by the time the second pump pulse arrives, which consequently changes the nature of nonlinear interferences. This then results in a significantly different final state, as can be seen, compared to the obtained vacuum state in the case
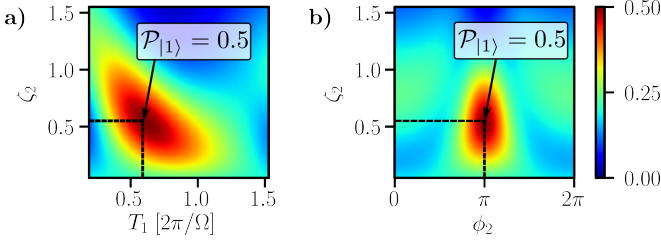
FIG. 2. **(a)** Probability of having a single photon in the signal mode in a two-pulse configuration, as a function of the parametric gain magnitude ζ_2 and delay time T_1 of the second pump pulse (fixed relative phase, $\phi_2 = \pi$ and $\phi_1 = 0$); **(b)** The same probability as a function of the phase and magnitude of $r_2 = \zeta_2\, e^{i\phi_2}$ (delay time fixed to $T_1 = 0.61\frac{2\pi}{\Omega}$). In both cases, the gain of the first pulse is $r_1 \approx 0.58$.

without the 2LS. Interestingly, we can see in Fig. 1(e), that the probability of generating a single pair of signal and idler photons reaches a value close to 0.5, which is twice the value than can be achieved in a conventional TMSV source, as was seen in Fig. 1(b).

In fact, the final state varies significantly with the parametric gain, relative phase, and the delay time between the pump pulses. To see this, in Fig. 2, we show the probability of finding a single-photon state in the signal mode (calculated by adding the probabilities of the $|1,1,g\rangle$ and $|0,1,e\rangle$ states): (a) as a function of the delay time T_1 and gain magnitude ζ_2 of the second pulse, for a fixed relative phase $\phi_2 - \phi_1 = \pi$; (b) as a function of the phase ϕ_2 and magnitude ζ_2 of the parametric gain of the second pulse, for a fixed delay time $T_1 = 0.61\frac{2\pi}{\Omega}$. The other parameters were identical to the configuration in Figs. 1(e,f). In Fig. 2(a), we see that the single-photon generation probability attains a maximum of 0.5 for a delay of $T_1 = 0.61\frac{2\pi}{\Omega}$ and a parametric gain of $\zeta_2 \approx 0.55$. In Fig. 2(b), we see that phases $\phi_2 \neq \pi$ always result in a lower single-photon generation probability. Further simulations (see Supplementary [31]) also showed that, within the considered ranges of ζ_2 and T_1, the highest single-photon probabilities are always obtained for a relative phase of π between two consecutive pump pulses.

Three-pulse configuration. While the high-dimensional space of control parameters in a multi-pulse sequence offers many ways to tune desired outputs, even configurations with a limited number of varying parameters are capable of generating high-photon-number Fock states, with generation probabilities far surpassing what is possible in a conventional TMSV source. To demonstrate this, we calculate the output for a configuration with three pump pulses. We use the parametric gains and delay times of the pulses as "control knobs" for tuning the system towards desired final states, namely to maximize the generation probability of different Fock states in the signal mode of the cavity. We fixed the relative phase between the pump pulses to π, such that $\phi_1 = 0$, $\phi_2 = \pi$,

and $\phi_3 = 0$. This choice is guided by our study shown in Fig. 2, to maximize the single-photon probability in the signal mode. This does not necessarily mean that this phase choice is a global optimum for maximizing the generation probability of other Fock states, yet it is a reasonable choice, and mainly an attempt to limit the space of control parameters in our optimization study.

For the parametric gain magnitudes, we consider values of $\zeta \leq 15$dB, which are experimentally achievable in TMSV sources [5]. From this point onward, we express parametric gain magnitudes in units of dB, calculated as $\zeta[\text{dB}] = -10\log_{10}(e^{-2\zeta})$, for easier comparison with experimental works on TMSV sources. We also restrict the total interaction time to $\leq 3\frac{2\pi}{\Omega}$, as the duration of coherent interactions between a quantum emitter and an optical cavity is limited in practice [33]. In the next section, we will briefly address the feasibility of realizing our optimized pulse sequences, in terms of the required interaction time, with respect to such realistic effects.
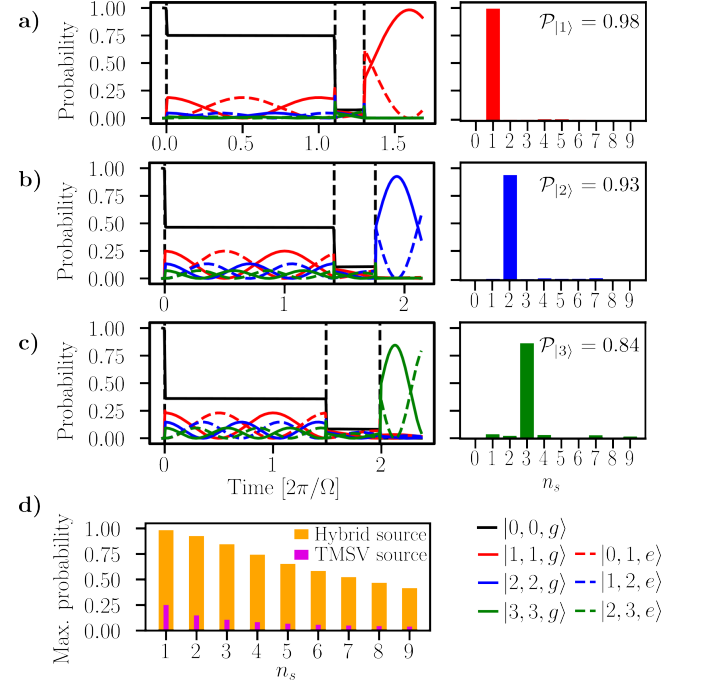

FIG. 3. **(a-c)** Left panels: Temporal evolution of probabilities in a configuration with three pump pulses, optimized for achieving maximum generation probability of (a) 1, (b) 2, and (c) 3 photons in the signal mode. The second pulse has a relative phase of π compared to the other two and the parametric gain of each pulse is indicated in each figure as ζ_j. Right panels: The corresponding photon-number probability distributions in the signal mode at the output. **(d)** The maximum obtained probabilities for generating photon number states $|1\rangle$ to $|9\rangle$ in the signal mode, in the three pulse configuration (yellow bars), and the maximum fundamentally attainable probabilities for generating the $|n, n\rangle$ states in a conventional TMSV source (purple bars).

Under the expressed boundary conditions for our

optimization with three pump pulses, we show in Figs. 3(a,b,c), the pulse configurations that result in the maximum achievable generation probability for the Fock states $|1\rangle$, $|2\rangle$ and $|3\rangle$ in the signal mode, respectively. The probability of generating an n-photon Fock state in the signal mode is calculated from summing up the mutually exclusive probabilities of generating the $|n, n, g\rangle$ and $|n-1, n, e\rangle$ states. As the signal mode does not interact with the 2LS, the Fock state in it can eventually escape a realistic cavity of finite quality factor for further utilization. The left panels in Figs. 3(a-c) show the temporal evolution of the probabilities, while the right panels show the final distribution of the probabilities for the signal-mode Fock states, where we find very high probabilities for generation of these distinct Fock states. Especially Figs. 3(a,b), show a near-on-demand generation of single- and two-photon Fock states, with 0.98 and 0.93 probabilities, respectively. In Fig. 3(d), we show the maximum probabilities for generation of Fock states with photon numbers up to $n_s = 9$, that can be obtained in our three-pulse optimization. With it, we also show the corresponding maximum probabilities attainable using a conventional TMSV source for comparison, which clearly demonstrates the enhancement achieved in the hybrid system. As an example, the probability for generating the $n_s = 9$ state is enhanced more than 10-fold compared to the TMSV source. The exact pulse sequence parameters for attaining each of the Fock states shown in Fig. 3(d) are given in the Supplementary [31].

Effects of loss. The obtained results up to now are only strictly valid in an idealized system, with no cavity losses, 100% coupling of the 2LS radiation into the cavity mode, and no internal dephasing of the 2LS, which

are not fully achievable in practice [33]. Longer interaction times, give more time to these effects to negatively affect the system dynamics. To take the first step into investigating our scheme under non-ideal conditions, we focus on the effects of having a finite quality factor for the cavity. We assume equal losses for both signal and idler cavity modes, characterized by the decay rate γ_c, and solve the Lindblad master equation $\partial_t \hat{\rho} = \frac{1}{i\hbar}[\hat{H}, \rho] - \sum_j \frac{1}{2}(\hat{c}_j^\dagger \hat{c}_j \rho + \rho \hat{c}_j^\dagger \hat{c}_j - 2\hat{c}_j \rho \hat{c}_j^\dagger)$, where $\hat{c}_j = \sqrt{\gamma_c} \hat{a}_j$ with $j = \{i, s\}$ are the jump operators [33]. We simulated the lossy hybrid system for the same sets of pump parameters as in Fig. 3(a-c). The results are shown in Fig. 4, where we only show the temporal evolution of the $|1, 1, g\rangle$ [(a)], $|2, 2, g\rangle$ [(b)], and $|3, 3, g\rangle$ [(c)] states for three values of the decay rate $\gamma_c = \{0.001, 0.008, 0.03\}\Omega$. As expected, the cavity loss reduces the probabilities of obtaining the target states, with the higher-order states suffering more due to their higher photon number. To emphasize this, the probabilities for obtaining a Fock state with $n_s = 1, 2, 3$ photons in the signal mode immediately after the third pulse are shown in Fig. 4(d), where each set of bars corresponds to a particular value of γ_c and the values shown are obtained by tracing-out the idler and 2LS degrees of freedom. In the supplementary [31], we present a rough calculation to connect the used γ_c values to the Purcell factor of an optical cavity, considering common range of solid-sate-emitter parameters for the 2LS [17, 33, 34], where in our estimation, state-of-the-art micro/nanostructured optical cavities can reach these requirements [35–37].

Discussion and conclusion. Our results are obtained by considering only a portion of the full control-parameter space of the hybrid system. Further expanding the search to include more pulses, continuous relative phase variations, higher parametric gains, and frequency detuning between the cavity modes and the 2LS, could lead to further enhancing the generation probabilities, to potentially reach near-deterministic generation of higher Fock states, or even other classes of non-Gaussian states for continuous variable quantum information processing [38]. Moreover, we only investigated loss with configurations optimized under lossless conditions. With an optimization under lossy conditions, one might identify pulse sequences that make the process more robust to losses.

Importantly, the hybrid source inherits the tunability of a TMSV source. Specially, the frequency spectrum of the output photons in the signal mode can be fully controlled by the energy conservation relation $\omega_s = \omega_p - \omega_0$, only by tuning the frequency spectrum of the pump pulses and the resonances of the nonlinear cavity, even while the 2LS is unchanged. This opens the door to fundamentally new opportunities for optical quantum technologies, starting with near-deterministic generation of Fock states for different applications in quantum computing, communication, and sensing, which commonly operate in very different wavelength ranges. Moreover,
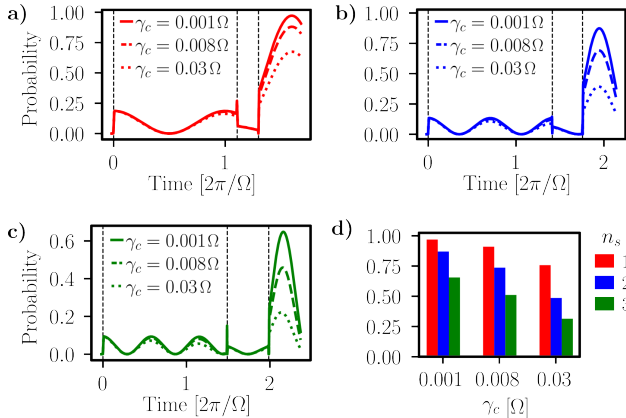

FIG. 4. **(a-c)** Temporal evolution of the $|1, 1, g\rangle$ (red), $|2, 2, g\rangle$ (blue), and $|3, 3, g\rangle$ (green) states in the presence of different amounts of cavity losses, quantified by γ_c, the decay rate for both the signal and idler modes. The pump configuration for each of the plots is identical to the corresponding optimized lossless cases shown in Fig. 3; **(d)** The probabilities of detecting $n_s = 1, 2, 3$ photons in the signal mode immediately after the third pump pulse.

with this scheme, one could in principle realize many indistinguishable sources of Fock states by using many frequency-distinguishable solid-state emitters [17].

Finally, although we had photonic systems in mind, the predicted dynamics are independent of the frequency range of operation and could potentially be adapted to other quantum information processing platforms, e.g. for microwave quantum-state generation in superconducting circuits [39, 40], motional quantum-state generation in trapped ions [41, 42], and generating phonon-photon excitations in optomechanical systems [43].

————————

* aleksa.krstic@uni-jena.de

[1] F. Flamini, N. Spagnolo, and F. Sciarrino, Photonic quantum information processing: a review, Reports on Progress in Physics **82**, 016001 (2018).

[2] C. Weedbrook, S. Pirandola, R. García-Patrón, N. J. Cerf, T. C. Ralph, J. H. Shapiro, and S. Lloyd, Gaussian quantum information, Reviews of Modern Physics **84**, 621 (2012).

[3] D. J. Brod, E. F. Galvão, A. Crespi, R. Osellame, N. Spagnolo, and F. Sciarrino, Photonic implementation of boson sampling: a review, Advanced Photonics **1**, 034001 (2019).

[4] M. Perarnau-Llobet, A. González-Tudela, and J. I. Cirac, Multimode fock states with large photon number: effective descriptions and applications in quantum metrology, Quantum Science and Technology **5**, 025003 (2020).

[5] H. Vahlbruch, M. Mehmet, K. Danzmann, and R. Schnabel, Detection of 15 db squeezed states of light and their application for the absolute calibration of photoelectric quantum efficiency, Physical Review Letters **117**, 110801 (2016).

[6] L. Barsotti, J. Harms, and R. Schnabel, Squeezed vacuum states of light for gravitational wave detectors, Reports on Progress in Physics **82**, 016905 (2018).

[7] P. Solano, Deterministic generation of large fock states, Physical Review Letters **125**, 093603 (2020).

[8] K. R. Brown, K. M. Dani, D. M. Stamper-Kurn, and K. B. Whaley, Deterministic optical fock-state generation, Phys. Rev. A **67**, 043818 (2003).

[9] A. González-Tudela, V. Paulisch, D. E. Chang, H. J. Kimble, and J. I. Cirac, Deterministic generation of arbitrary photonic states assisted by dissipation, Phys. Rev. Lett. **115**, 163603 (2015).

[10] M. Cosacchi, J. Wiercinski, T. Seidelmann, M. Cygorek, A. Vagov, D. E. Reiter, and V. M. Axt, On-demand generation of higher-order fock states in quantum-dot–cavity systems, Phys. Rev. Res. **2**, 033489 (2020).

[11] F. Lenzini, B. Haylock, J. C. Loredo, R. A. Abrahao, N. A. Zakaria, S. Kasture, I. Sagnes, A. Lemaitre, H.-P. Phan, D. V. Dao, *et al.*, Active demultiplexing of single photons from a solid-state source, Laser & Photonics Reviews **11**, 1600297 (2017).

[12] H. Wang, J. Qin, X. Ding, M.-C. Chen, S. Chen, X. You, Y.-M. He, X. Jiang, L. You, Z. Wang, C. Schneider, J. J. Renema, S. Höfling, C.-Y. Lu, and J.-W. Pan, Boson sampling with 20 input photons and a 60-mode interferometer in a 10^{14}-dimensional hilbert space, Phys. Rev. Lett. **123**, 250503 (2019).

[13] L. M. Hansen, L. Carosini, L. Jehle, F. Giorgino, R. Houvenaghel, M. Vyvlecka, J. C. Loredo, and P. Walther, Single-active-element demultiplexed multiphoton source, Optica Quantum **1**, 1 (2023).

[14] E. Waks, E. Diamanti, and Y. Yamamoto, Generation of photon number states, New Journal of Physics **8**, 4 (2006).

[15] M. Cooper, L. J. Wright, C. Söller, and B. J. Smith, Experimental generation of multi-photon fock states, Optics express **21**, 5309 (2013).

[16] J. Tiedau, T. J. Bartley, G. Harder, A. E. Lita, S. W. Nam, T. Gerrits, and C. Silberhorn, Scalability of parametric down-conversion for generating higher-order fock states, Physical Review A **100**, 041802 (2019).

[17] J. Lee, V. Leong, D. Kalashnikov, J. Dai, A. Gandhi, and L. A. Krivitsky, Integrated single photon emitters, AVS Quantum Science **2** (2020).

[18] Y. Wang, K. D. Jöns, and Z. Sun, Integrated photon-pair sources with nonlinear optics, Applied Physics Reviews **8** (2021).

[19] W. Qin, A. Miranowicz, P.-B. Li, X.-Y. Lü, J.-Q. You, and F. Nori, Exponentially enhanced light-matter interaction, cooperativities, and steady-state entanglement using parametric amplification, Physical Review Letters **120**, 093601 (2018).

[20] C. Leroux, L. C. G. Govia, and A. A. Clerk, Enhancing cavity quantum electrodynamics via antisqueezing: Synthetic ultrastrong coupling, Phys. Rev. Lett. **120**, 093602 (2018).

[21] S. Saravi, A. N. Poddubny, T. Pertsch, F. Setzpfandt, and A. A. Sukhorukov, Atom-mediated spontaneous parametric down-conversion in periodic waveguides, Optics Letters **42**, 4724 (2017).

[22] L. Ping, W. Li, C. Zhu, Y. Yang, and G. Agarwal, Parametric-interaction-induced avoided dressed-state crossings in cavity qed: Generation of quantum coherence and equally weighted superposition of fock states, Physical Review Research **4**, 013014 (2022).

[23] Y.-H. Chen, W. Qin, X. Wang, A. Miranowicz, and F. Nori, Shortcuts to adiabaticity for the quantum rabi model: Efficient generation of giant entangled cat states via parametric amplification, Physical Review Letters **126**, 023602 (2021).

[24] B. L. Schumaker and C. M. Caves, New formalism for two-photon quantum optics. ii. mathematical foundation and compact notation, Physical Review A **31**, 3093 (1985).

[25] A. Eckstein, A. Christ, P. J. Mosley, and C. Silberhorn, Highly efficient single-pass source of pulsed single-mode twin beams of light, Physical Review Letters **106**, 013603

(2011).

[26] E. Meyer-Scott, C. Silberhorn, and A. Migdall, Single-photon sources: Approaching the ideal through multiplexing, Review of Scientific Instruments **91**, 041101 (2020).

[27] S. Saravi, T. Pertsch, and F. Setzpfandt, Lithium niobate on insulator: an emerging platform for integrated quantum photonics, Advanced Optical Materials **9**, 2100789 (2021).

[28] M. O. Scully and M. S. Zubairy, *Quantum Optics* (Cambridge University Press, 1997).

[29] E. T. Jaynes and F. W. Cummings, Comparison of quantum and semiclassical radiation theories with application to the beam maser, Proceedings of the IEEE **51**, 89 (1963).

[30] J. R. Johansson, P. D. Nation, and F. Nori, QuTiP: An open-source Python framework for the dynamics of open quantum systems, Computer Physics Communications **183**, 1760 (2012).

[31] See Supplemental Material at [URL-will-be-inserted-by-publisher].

[32] M. V. Chekhova and Z. Y. Ou, Nonlinear interferometers in quantum optics, Advances in Optics and Photonics **8**, 104 (2016).

[33] P. Lodahl, S. Mahmoodian, and S. Stobbe, Interfacing single photons and single quantum dots with photonic nanostructures, Rev. Mod. Phys. **87**, 347 (2015).

[34] Y.-M. He, G. Clark, J. R. Schaibley, Y. He, M.-C. Chen, Y.-J. Wei, X. Ding, Q. Zhang, W. Yao, X. Xu, *et al.*, Single quantum emitters in monolayer semiconductors, Nature nanotechnology **10**, 497 (2015).

[35] P. B. Deotare, M. W. McCutcheon, I. W. Frank, M. Khan, and M. Lončar, High quality factor photonic crystal nanobeam cavities, Applied Physics Letters **94**

(2009).

[36] B. Merkel, A. Ulanowski, and A. Reiserer, Coherent and purcell-enhanced emission from erbium dopants in a cryogenic high-q resonator, Phys. Rev. X **10**, 041025 (2020).

[37] A. Barreda, L. Mercadé, M. Zapata-Herrera, J. Aizpurua, and A. Martínez, Hybrid photonic-plasmonic cavity design for very large purcell factors at telecommunication wavelengths, Phys. Rev. Appl. **18**, 044066 (2022).

[38] M. Walschaers, Non-gaussian quantum states and where to find them, PRX Quantum **2**, 030204 (2021).

[39] C. Rolland, A. Peugeot, S. Dambach, M. Westig, B. Kubala, Y. Mukharsky, C. Altimiras, H. le Sueur, P. Joyez, D. Vion, P. Roche, D. Esteve, J. Ankerhold, and F. Portier, Antibunched photons emitted by a dc-biased josephson junction, Phys. Rev. Lett. **122**, 186804 (2019).

[40] A. Peugeot, G. Ménard, S. Dambach, M. Westig, B. Kubala, Y. Mukharsky, C. Altimiras, P. Joyez, D. Vion, P. Roche, D. Esteve, P. Milman, J. Leppäkangas, G. Johansson, M. Hofheinz, J. Ankerhold, and F. Portier, Generating two continuous entangled microwave beams using a dc-biased josephson junction, Phys. Rev. X **11**, 031008 (2021).

[41] D. M. Meekhof, C. Monroe, B. E. King, W. M. Itano, and D. J. Wineland, Generation of nonclassical motional states of a trapped atom, Phys. Rev. Lett. **76**, 1796 (1996).

[42] W. Ge, B. C. Sawyer, J. W. Britton, K. Jacobs, J. J. Bollinger, and M. Foss-Feig, Trapped ion quantum information processing with squeezed phonons, Phys. Rev. Lett. **122**, 030501 (2019).

[43] S. Barzanjeh, A. Xuereb, S. Gröblacher, M. Paternostro, C. A. Regal, and E. M. Weig, Optomechanics for quantum technologies, Nature Physics **18**, 15 (2022).

A hybrid source of quantum light for generation of frequency tunable Fock states

Aleksa Krstić,[1, *] Priyanshu Tiwari,[1] Florian Höhe,[2] Frank
Setzpfandt,[1, 3] Ulf Peschel,[4] Joachim Ankerhold,[2] and Sina Saravi[1]

[1]*Institute of Applied Physics, Abbe Center of Photonics,*
Friedrich-Schiller University Jena, Albert-Einstein-Straße 15, 07745 Jena, Germany
[2]*Institute for Complex Quantum Systems and IQST,*
University of Ulm, Albert-Einstein-Allee 11, 89069 Ulm, Germany
[3]*Fraunhofer Institute for Applied Optics and Precision Engineering, Albert-Einstein-Straße 7, 07745 Jena, Germany*
[4]*Institute of Condensed Matter Theory and Solid State Optics,*
Friedrich-Schiller University Jena, Max-Wien-Platz 1, 07743 Jena, Germany
(Dated: April 25, 2024)

CONTENTS

S1. THE INTERACTION HAMILTONIAN

The nonlinear interaction inside the crystal and the interaction of the emitter with the idler mode are described by the total Hamiltonian $\hat{H}(t) = \hat{H}_0 + \hat{H}_{\mathrm{NL}}(t) + \hat{H}_{\mathrm{JC}}$. Here, $\hat{H}_{\mathrm{NL}}(t) = \hbar\Gamma\mathcal{E}(t)\,e^{-i\omega_p t}\hat{a}_i^\dagger\hat{a}_s^\dagger + $ H.c. is the Hamiltonian of a two-mode parametric amplifier excited by monochromatic pump pulses of frequency ω_p, $\hat{a}_i$ and $\hat{a}_s$ are the annihilation operators for the idler and signal modes, respectively, Γ is the nonlinear coupling constant and $\mathcal{E}(t)$ is the temporal envelope of the pump pulses; $\hat{H}_{\mathrm{JC}} = i\hbar\frac{\Omega}{2}\hat{a}_i\hat{\sigma}^\dagger + $ H.c. is the Jaynes-Cummings (JC) Hamiltonian, where Ω is the single-photon Rabi frequency and $\hat{\sigma}$ is the atomic lowering operator [S1]; finally, $\hat{H}_0 = \hbar(\omega_i\hat{a}_i^\dagger\hat{a}_i + \omega_s\hat{a}_s^\dagger\hat{a}_s) + \hbar\omega_0\hat{\sigma}^\dagger\hat{\sigma}$ contains the free Hamiltonians of the cavity modes and the emitter. As both the nonlinear and JC interactions are assumed to be resonant (with $\omega_0 = \omega_i$ and $\omega_p = \omega_i + \omega_s$), after we transition into the interaction picture via the transformation $\hat{U}_0 = e^{-\frac{i}{\hbar}\hat{H}_0 t}$, the total interaction Hamiltonian takes the form

$$\hat{H}(t) = \hbar\Gamma\mathcal{E}(t)\hat{a}_i^\dagger\hat{a}_s^\dagger + i\hbar\Omega\hat{a}_i\hat{\sigma}^\dagger + \text{ H.c.} \tag{S1}$$

S2. EFFECTS OF PUMP RELATIVE PHASE IN A TWO-PULSE CONFIGURATION

As discussed in the main text, the relative phase between the pump pulses exciting the nonlinear cavity is one of the parameters that influences the final distribution of multi-pair states at the output of the hybrid source. In the two-pulse example in Fig. 2(b), we showed the dependence of the probability of obtaining a single photon in the signal mode as a function of the magnitude ζ_2 and phase ϕ_2 of the parametric gain of the second pump pulse, for a fixed delay time T_1. For the set of parameters and parameter ranges investigated, the single photon probability exhibits a maximum for $\phi_2 = \pi$. While our simulations indicate (as will be shown here) that a **global** maximum for the three parameters considered $\{\zeta_2, \phi_2, T_1\}$ is always attained for $\phi_2 = \pi$, the single photon probability can exhibit local maxima at different values of ϕ_2, when T_1 is varied. This behavior is shown in Fig. S1, where we see that the single

---

photon probability (again calculated by adding the probabilities of the $|1, 1, g\rangle$ and $|0, 1, e\rangle$ states) can exhibit either a single maximum for $\phi_2 = \pi$ at shorter T_1, or multiple maxima at $\phi_2 \neq \pi$ at longer T_1, with the exact value of T_1 at which the behavior changes depending on the value of ζ_2. Regardless of ζ_2, the single maximum at $\phi_2 = \pi$ is always the highest value.
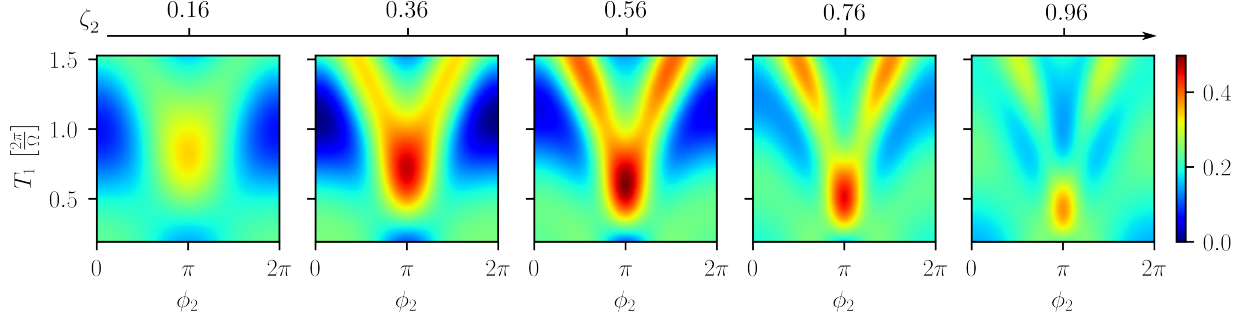

Figure S1. The probability of having a single photon in the signal mode in a two pulse configuration, as a function of the parametric gain phase ϕ_2 and delay time T_1 of the second pulse. The second pulse has a fixed gain magnitude ζ_2 for each plot, with the value increasing from left to right, as indicated by the axis above the figures. In all cases the gain of the first pulse is fixed to $r_1 \approx 0.58$.

S3. SYSTEM DYNAMICS AND NUMERICAL PROCEDURES

In order to efficiently perform a sweep of parameters, to evaluate the possible output states for the three-pulse configuration discussed in the main text, we make use of the assumption that the duration of each pump pulse is much shorter than the few-photon Rabi periods of the 2LS. As we will show here, this allows the nonlinear and 2LS dynamics to be evaluated separately and avoids the need for integrating the full Schrödinger equation for each set of pulse parameters.

In the interaction picture, the evolution operator of the hybrid system is written as

$$\hat{U}(t) = \mathcal{T} \exp \left[-\frac{i}{\hbar} \int_{-\infty}^{t} dt' \, \hat{H}(t') \right], \tag{S2}$$

where, $\hat{H}(t')$ is given by Eq. S1 and $\mathcal{T}$ indicates the time-ordering superoperator. By expanding the interaction Hamiltonian according to Eq. S1 we obtain

$$\hat{U}(t) = \mathcal{T} \exp \left\{ -\frac{i}{\hbar} \int_{-\infty}^{t} dt' \left[\hbar \Gamma \mathcal{E}(t') \hat{a}_i^\dagger \hat{a}_s^\dagger + i\hbar \Omega \hat{a}_i \hat{\sigma}^\dagger + \text{H.c.} \right] \right\}. \tag{S3}$$

We now assume that the pump field envelope $\mathcal{E}(t')$ consists of a sequence of temporally distinct pulses as $\mathcal{E}(t') = \sum_j \mathcal{E}_j(t')$, where $\mathcal{E}_j(t') = |\mathcal{E}_j(t')| e^{i\phi_j}$ is the envelope of the j-th pulse consisting of a time-dependent amplitude $|\mathcal{E}_j(t')|$ and arbitrary *time-independent* phase ϕ_j.

We can divide the total interaction time into intervals during a pump pulse, of duration δT_j, and intervals in-between pulses, of duration T_j. In-between the j-th and $j+1$-th pulses, we have $\mathcal{E}(t) \approx 0$ and can neglect the nonlinear interaction, thus, the evolution over that time interval is well approximated by

$$\hat{U}_{2\text{LS}}^{(j)} = \exp \left[T_j \Omega \hat{a}_i \hat{\sigma}^\dagger - \text{H.c.} \right]. \tag{S4}$$

For intervals during a pulse, the assumption $\delta T_j \ll \frac{2\pi}{\Omega}$ results in the contributions from the 2LS interaction being negligible in comparison to the nonlinear interaction. Thus, the evolution of the system due to the j-th pump pulse is well-approximated by $\hat{U}_{\text{NL}}^{(j)} = \mathcal{T} \exp \left\{ -i\Gamma \int_j dt' \left[\mathcal{E}_j(t') \hat{a}_i^\dagger \hat{a}_s^\dagger + \mathcal{E}_j^*(t') \hat{a}_i \hat{a}_s \right] \right\}$. The form of $\hat{U}_{\text{NL}}^{(j)}$ can be further simplified by recalling $\mathcal{E}_j(t') = |\mathcal{E}_j(t')| e^{i\phi_j}$ and rewriting the integrand in the exponential as $|\mathcal{E}_j(t')| \left(e^{i\phi_j} \hat{a}_i^\dagger \hat{a}_s^\dagger + e^{-i\phi_j} \hat{a}_i \hat{a}_s \right)$, which leaves the operator part of the integrand *time-independent* and eliminates the need for explicit time-ordering in the expression for $\hat{U}_{\text{NL}}^{(j)}$, which takes on the form

$$\hat{U}_{\text{NL}}^{(j)} = \exp \left[-i \left(r_j \hat{a}_i^\dagger \hat{a}_s^\dagger + r_j^* \hat{a}_i \hat{a}_s \right) \right], \tag{S5}$$

where we defined $r_j = \Gamma \int_j dt' \mathcal{E}_j(t')$. This operator has the exact form of a two-mode squeezing operator with the parametric gain $r_j = \zeta_j e^{i\phi_j}$ [S2] and generates a TMSV state when acting on a vacuum initial state. Another consequence of the definition Eq. S5 is that the nonlinear part of the evolution is completely described by the parametric gain associated with the pulse and the exact shape of the pulse does not affect the result.

By taking into account the above conclusions, the total evolution operator of the hybrid system up to the time t, excited by a series of temporally-distinct pulses can be represented as

$$\hat{U}(t) \approx \prod_j \hat{U}_{2\text{LS}}^{(j)} \hat{U}_{\text{NL}}^{(j)}, \tag{S6}$$

where the pairs of operators are ordered from left to right in descending order with respect to j.

In order to efficiently evaluate the state at the output of a large set of pump pulse configurations, we calculated the matrix representation of $\hat{U}_{2\text{LS}}^{(j)}$ and $\hat{U}_{\text{NL}}^{(j)}$ in a sufficiently large basis set and sequentially applied them to the initial state $|0, 0, g\rangle$. The process was repeated for all combinations of pulse parameters involved, i.e. $\{\zeta_1, T_1, \zeta_2, T_2, \zeta_3\}$, to obtain the various parameter dependencies shown in Figs. 2 and S1, as well as to find the optimal configurations for the particular Fock states, whose temporal evolution is shown in Fig. 3. In all of the aforementioned cases, we found that a composite basis $\{|n, n, g\rangle, |n-1, n, e\rangle\}$ with up to $n = 60$ represents a good balance between numerical accuracy and computation time. Yet, we note, that this number depends on the total parametric gain that the system experiences and a larger composite basis should be used if higher gain magnitudes or more pulses are considered.

Once the optimum pulse configurations were found using the above-explained method, we obtained and plotted the temporal evolution of the system for particular pulse configurations. This was done using the `QuTiP` library in Python [S3], both to solve the Schrödinger equation for the lossless system (shown in Figs. 1 and 3) and to solve the Lindblad master equation in the lossy system (shown in Fig. 4). Finally, in the table below, we show the optimal three-pulse-configuration parameters, corresponding to the maximum probabilities for obtaining the Fock states with up to $n_s = 9$, shown in Fig. 3(d).

Fock state	$\mathcal{P}$	ζ_1 [dB]	T_1 $[\frac{2\pi}{\Omega}]$	ζ_2 [dB]	T_2 $[\frac{2\pi}{\Omega}]$	ζ_3 [dB]
$|1\rangle$	0.98	4.76	1.11	12.86	0.19	12.39
$|2\rangle$	0.93	8.10	1.41	12.86	0.34	10.96
$|3\rangle$	0.85	9.53	1.49	13.34	0.50	10.00
$|4\rangle$	0.74	9.53	1.49	13.34	0.65	9.53
$|5\rangle$	0.65	8.57	1.49	13.34	0.80	9.05
$|6\rangle$	0.58	8.57	1.49	13.34	0.95	8.57
$|7\rangle$	0.52	9.05	1.49	13.34	1.11	8.10
$|8\rangle$	0.47	9.53	1.49	13.34	1.26	7.62
$|9\rangle$	0.42	10.00	1.49	13.34	1.41	7.15

Table S1. The maximum probabilities and corresponding parameter values for the optimal pump pulse configurations for generating Fock states up to $n_s = 9$ in the three-pulse configuration.

S4. ESTIMATION OF PURCELL FACTOR FROM CAVITY DECAY RATE FOR REALISTIC OPTICAL SYSTEMS

We assume a spontaneous decay rate of $\Gamma_0 = 10^9 s^{-1}$ for the 2LS, which is in the same order of magnitude of many common solid-state quantum emitters [S4–S6]. With a center wavelength of the idler mode at $\lambda_0 = 600$nm, and a mode volume of $V = 10\lambda_0^3$ for the cavity, we find the single-photon Rabi frequency $\Omega = \sqrt{\frac{3c\Gamma_0 \lambda_0^2}{2\pi V}} \approx 1.6 \times 10^{11} \ s^{-1}$ [S7], and can use it to calculate the quality factors $Q = \frac{2\pi c}{\lambda_0 \gamma_c}$, associated with each of the values of γ_c. Thus, to achieve system dynamics corresponding to the solid lines in Fig. 4(a,b,c), we require a cavity with a quality factor of $Q \approx 1.9 \times 10^7$, while to obtain dynamics corresponding to the dashed and dotted lines, we require quality factors of $Q \approx 2.5 \times 10^6$ and $Q \approx 6.5 \times 10^5$, respectively. Although the range of investigated values of γ_c correspond to the strong coupling regime ($\gamma_c \ll \Omega$), we can calculate a Purcell factor for the cavity $F = \frac{3}{4\pi^2} \frac{Q}{V/\lambda^3}$ [S4], corresponding to these three Q values. We then find the values of $F \approx 5 \times 10^3$, $F \approx 1.9 \times 10^4$, and $F \approx 1.4 \times 10^5$ for the smallest to largest of the quality factors. We point out, that although these Purcell factors are quite large, they are within reach in realistic photonic structures, such as photonic crystal cavities [S8], fiber-based microcavities [S9], or hybrid-plasmonic cavities

[S10].

––––––––––––––––––––

[S1] E. T. Jaynes and F. W. Cummings, Comparison of quantum and semiclassical radiation theories with application to the beam maser, Proceedings of the IEEE **51**, 89 (1963).

[S2] B. L. Schumaker and C. M. Caves, New formalism for two-photon quantum optics. ii. mathematical foundation and compact notation, Physical Review A **31**, 3093 (1985).

[S3] J. R. Johansson, P. D. Nation, and F. Nori, QuTiP: An open-source Python framework for the dynamics of open quantum systems, Computer Physics Communications **183**, 1760 (2012).

[S4] P. Lodahl, S. Mahmoodian, and S. Stobbe, Interfacing single photons and single quantum dots with photonic nanostructures, Rev. Mod. Phys. **87**, 347 (2015).

[S5] Y.-M. He, G. Clark, J. R. Schaibley, Y. He, M.-C. Chen, Y.-J. Wei, X. Ding, Q. Zhang, W. Yao, X. Xu, *et al.*, Single quantum emitters in monolayer semiconductors, Nature nanotechnology **10**, 497 (2015).

[S6] J. Lee, V. Leong, D. Kalashnikov, J. Dai, A. Gandhi, and L. A. Krivitsky, Integrated single photon emitters, AVS Quantum Science **2** (2020).

[S7] M. O. Scully and M. S. Zubairy, *Quantum Optics* (Cambridge University Press, 1997).

[S8] P. B. Deotare, M. W. McCutcheon, I. W. Frank, M. Khan, and M. Lončar, High quality factor photonic crystal nanobeam cavities, Applied Physics Letters **94** (2009).

[S9] B. Merkel, A. Ulanowski, and A. Reiserer, Coherent and purcell-enhanced emission from erbium dopants in a cryogenic high-q resonator, Phys. Rev. X **10**, 041025 (2020).

[S10] A. Barreda, L. Mercadé, M. Zapata-Herrera, J. Aizpurua, and A. Martínez, Hybrid photonic-plasmonic cavity design for very large purcell factors at telecommunication wavelengths, Phys. Rev. Appl. **18**, 044066 (2022).